Ceramics International 48 (2022) 23307–23313

Contents lists available at ScienceDirect

Ceramics International

journal homepage: www.elsevier.com/locate/ceramint

Crystal structure and microwave dielectric properties of $(Mg_{0.2}Ni0_{.2}Zn_{0.2}Co_{0.2}Mn_{0.2})_2SiO_4$ - A novel high-entropy ceramic

Kui Liu [a,*], Huaiwu Zhang [a,b,**], Cheng Liu [a], Jie Li [a], Liang Shi [a], Xueying Wang [a], Dainan Zhang [a,b]

[a] School of Electronic Science and Engineering, University of Electronic Science and Technology of China, Chengdu, 610054, China
[b] State Key Laboratory of Electronic Thin Film and Integrated Devices, University of Electronic Science and Technology of China, Chengdu, 610054, China

ARTICLE INFO

Keywords:
High-entropy ceramic
Microwave dielectric properties
PVL theory
Octahedral distortion

ABSTRACT

Novel $(Mg_{0.2}Ni_{0.2}Zn_{0.2}Co_{0.2}Mn_{0.2})_2SiO_4$ (A5SO) high-entropy microwave dielectric ceramics with olivine structure were prepared in the sintering temperature range of 1100 °C–1300 °C via the solid-phase reaction route. The crystal structure was confirmed by XRD, Raman, and Rietveld refinement. Optimal microwave dielectric properties (ε_r = 8.02, tanδ = 0.00051 at 14.5 GHz, and τ_f = −38.2 ppm/°C) were obtained at the sintering temperature of 1250 °C, where a relative density of 95.1% was detected. The complex chemical bonding theory manifests that the ε_r value of A5SO is mainly affected by the ionicity of A-O (A = Mg, Ni, Zn, Co, Mn) bond, while the dielectric loss is affected by both A-O and Si–O lattice energy. The τ_f value is mainly influenced by the [A(2)O_6] oxygen octahedral distortion (1.8×10^{-3}). The experimental results of this study provide both theoretical and practical guidance for high-entropy microwave dielectric ceramic applications.

1. Introduction

Microwave dielectric ceramics play an important role in wireless communication technology. The 5G/6G communication technology with greater capacity and shorter delay has put more stringent requirements on microwave dielectric ceramics performance. Typically, dielectric materials applied for high frequency need to have a low relative permittivity (ε_r < 15), low dielectric loss, and a near-zero temperature coefficient of resonance frequency τ_f [1–3]. Currently, It was reported that aluminates, borates, phosphates, molybdates, tungstates, and silicates usually possess low relative permittivity and low dielectric loss [4–12], but their inferior thermal stability limit their applications.

Recently, high Entropy Alloys (HEAs) have gradually become one of the solutions for designing materials with high performance more in line with the demand of the materials industry. The concept of high-entropy comes from the HEAs proposed in 2004, which is a single-phase solid solution formed by five or more metallic elements in one equimolar ratio [13,14]. The high-entropy, lattice distortion, hysteresis-diffusion, and cocktail effects are introduced to enhance its performance [15,16]. Therefore, studies on high-entropy ceramics, high-entropy glasses, high-entropy polymers were carried out [17,18]. According to the Gibbs free energy expression:

$$G = H\text{-}TS \quad (1)$$

where G is Gibbs free energy, H is enthalpy, T is temperature, and S is entropy. Materials with high entropy values are more stable at high temperatures [19,20]. Accordingly, the concept of high entropy is introduced into microwave dielectric ceramics for higher performance. A_2BO_4 (A = Mg, Zn, Ca; B=Si, Ge) with olivine structure has been widely studied as a representative of low permittivity families. Its derivative, $LiABO_4$ (A = Mg, Zn, Ca, Ln; B=Si, Ge), has also shown excellent dielectric properties [21–29]. Currently, Xiang et al. reported promising properties in $Li(Gd_{0.2}Ho_{0.2}Er_{0.2}Yb_{0.2}Lu_{0.2})GeO_4$ high-entropy microwave dielectric ceramics with rhombohedral olivine structure: ε_r = 7.2, tanδ = 0.00053, and τ_f = −2.9 ppm/°C [30]. Subsequent addition of 3 wt % H_3BO_3 as a sintering aid contributed to a reduced sintering temperature of 900 °C. However, its high preparation cost hinders its practical application. In contrast, olivine structured A_2SiO_4, is a low-cost solution and has significant advantages in realizing practical applications.

In this study, $(Mg_{0.2}Ni_{0.2}Zn_{0.2}Co_{0.2}Mn_{0.2})_2SiO_4$ (A5SO) microwave dielectric high-entropy ceramics were prepared by the solid-phase method. The relationship between he crystal structure and properties

* Corresponding author.
** Corresponding author. School of Electronic Science and Engineering, University of Electronic Science and Technology of China, Chengdu, 610054, China.
E-mail addresses: liukui96@163.com (K. Liu), hwzhang@uestc.edu.cn (H. Zhang).

https://doi.org/10.1016/j.ceramint.2022.04.317
Received 9 March 2022; Received in revised form 21 April 2022; Accepted 26 April 2022
Available online 29 April 2022

was investigated. It is expected that this study could provide theoretical and practical guidance for the high-entropy microwave dielectric ceramics.

2. Experimental

A5SO high-entropy ceramics were prepared from SiO_2 (Aladdin, 99%), MgO (Aladdin, 98%), NiO (Aladdin, 99%), ZnO (Aladdin, 99%), CoO (Aladdin, 99%), and MnO (Aladdin, 99.5%) by solid-phase reaction route. The flow diagram of preparation process is shown in Fig. 1. The raw materials were weighed according to the stoichiometric ratio and placed in a ball mill jar, and then ball milled in deionized water for 10 h (grinding media: zirconia balls). The dried powders were sieved at 120 mesh and placed in a muffle furnace for calcination at 900 °C for 6 h. Then the calcined powders were secondly ball-milled for 6 h, dried, and added 8 wt% polyvinyl alcohol aqueous solution (PVA) as a binder, and the powders were pressed into a cylindrical billet with a thickness of 5–6 mm and a diameter of 12 mm under the pressure of 10 MPa. Finally, the raw blanks were held at 500 °C for 2 h to exclude PVA and then heated up to 1100–1300 °C for 8 h of sintering in the air.

The crystal structure of prepared ceramics were analyzed through X-ray diffraction (XRD, Miniflex600, Rigaku, Japan) with Cu-Kα radiation from 10 to 90° at a step size of 0.02°. Raman spectroscopy was performed with a Raman microscope (InVia, Renishaw, UK) using an argon ion laser (λ = 532 nm) as the excitation light. Scanning electron microscopy (SEM, Phenom, Pharos, Netherlands) was used to observe the microscopic morphology. The apparent density was measured using the Archimedes method. A vector network analyzer (Agilent N5230A, Agilent Technologies, USA) was used to measure the microwave dielectric properties in TE011 mode using the Hakki-Coleman dielectric resonator method [31]. The resonant frequencies at different temperatures were calculated to obtain τ_f with the following eq.

$$\tau_f = \frac{f_{80} - f_{20}}{(T_{80} - T_{20}) \times f_{20}} \times 10^6 \ ppm \Big/ {}^{\circ}C \tag{2}$$

where f_{80} and f_{20} correspond to the resonant frequencies at 80 °C and 20 °C, respectively.

3. Results and discussion

Fig. 2(a) shows the XRD patterns of A5SO high-entropy ceramics sintered at different sintering temperatures. Comparing the characteristic peaks with olivine-type Mg_2SiO_4 (PDF#78–1371), Co_2SiO_4 (PDF#84–1298) and Mn_2SiO_4 (PDF#74–0716), it is indicated that the characteristic peaks of olivine-type A5SO high-entropy ceramics (space group: *Pbnm*, 62) lie between the characteristic peaks of Mg_2SiO_4 and Co_2SiO_4. Since the A5SO high entropy ceramics contain equimolar ratios of Mg^{2+} (ionic radius $r = 0.72$ Å), Ni^{2+} ($r = 0.69$ Å), Zn^{2+} ($r = 0.74$ Å), Co^{2+} ($r = 0.745$ Å), Mn^{2+} ($r = 0.83$ Å), which results in a variation of the lattice parameters. To further determine the lattice parameters of the A5SO high-entropy ceramics, the XRD data sintered at 1250 °C for 8 h were refined by Rietveld refinement using FULLPROF software, and the results are plotted in Fig. 2(b). The fitted curves agree well with the experimental data. The goodness of fit of refinement, which is defined as the ratio of R_{wp} *to* R_{exp}, is 1.81. Table 1 lists the refined lattice parameters and the corresponding theoretical densities of A5SO, as well as the data obtained from the PDF standard cards and literature for A_2SiO_4 (A = Mg, Ni, Co, Zn, Mn). The lattice parameters of A5SO calculated by Rietveld refinement are: $a = 4.7762$ Å, $b = 10.3609$ Å, $c = 6.0384$ Å, and

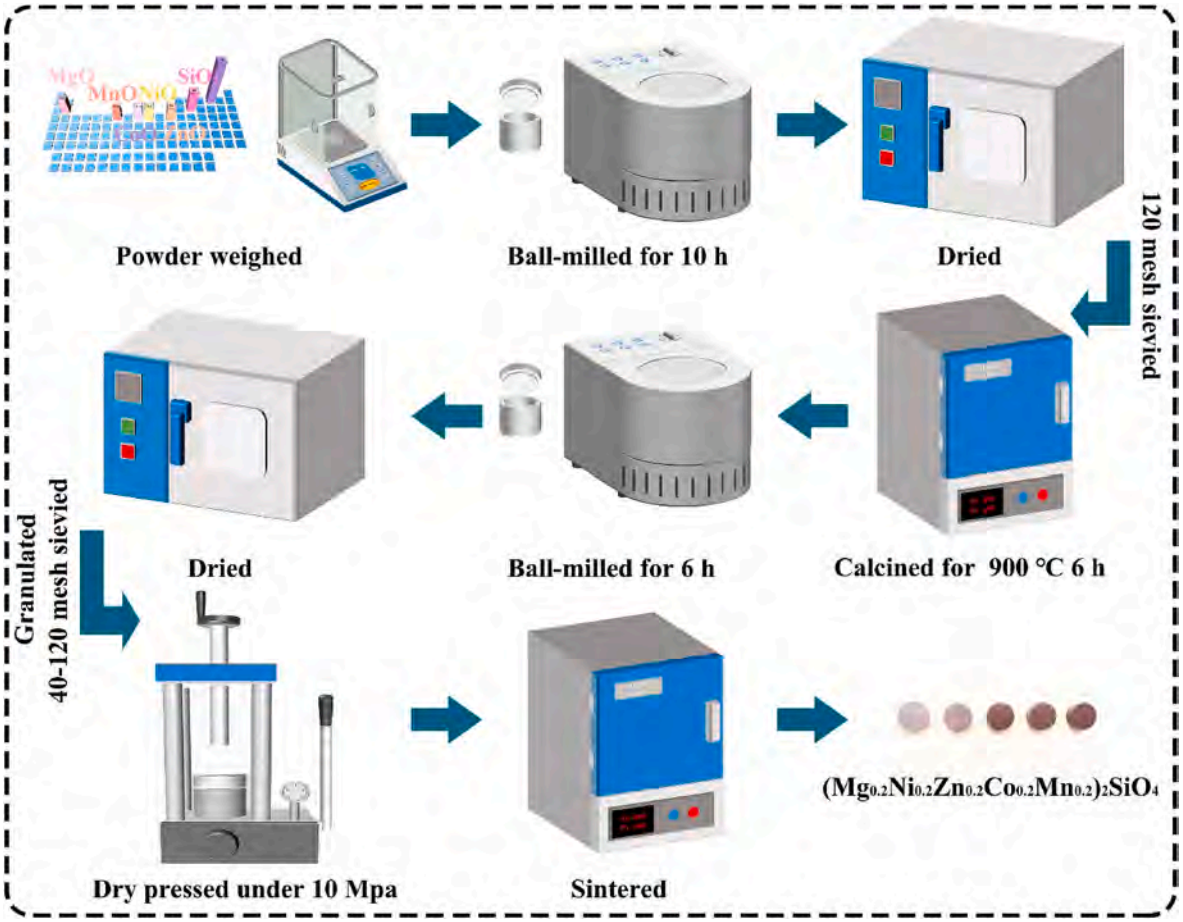

Fig. 1. Flow chart of the solid phase preparation of high-entropy microwave dielectric ceramics.

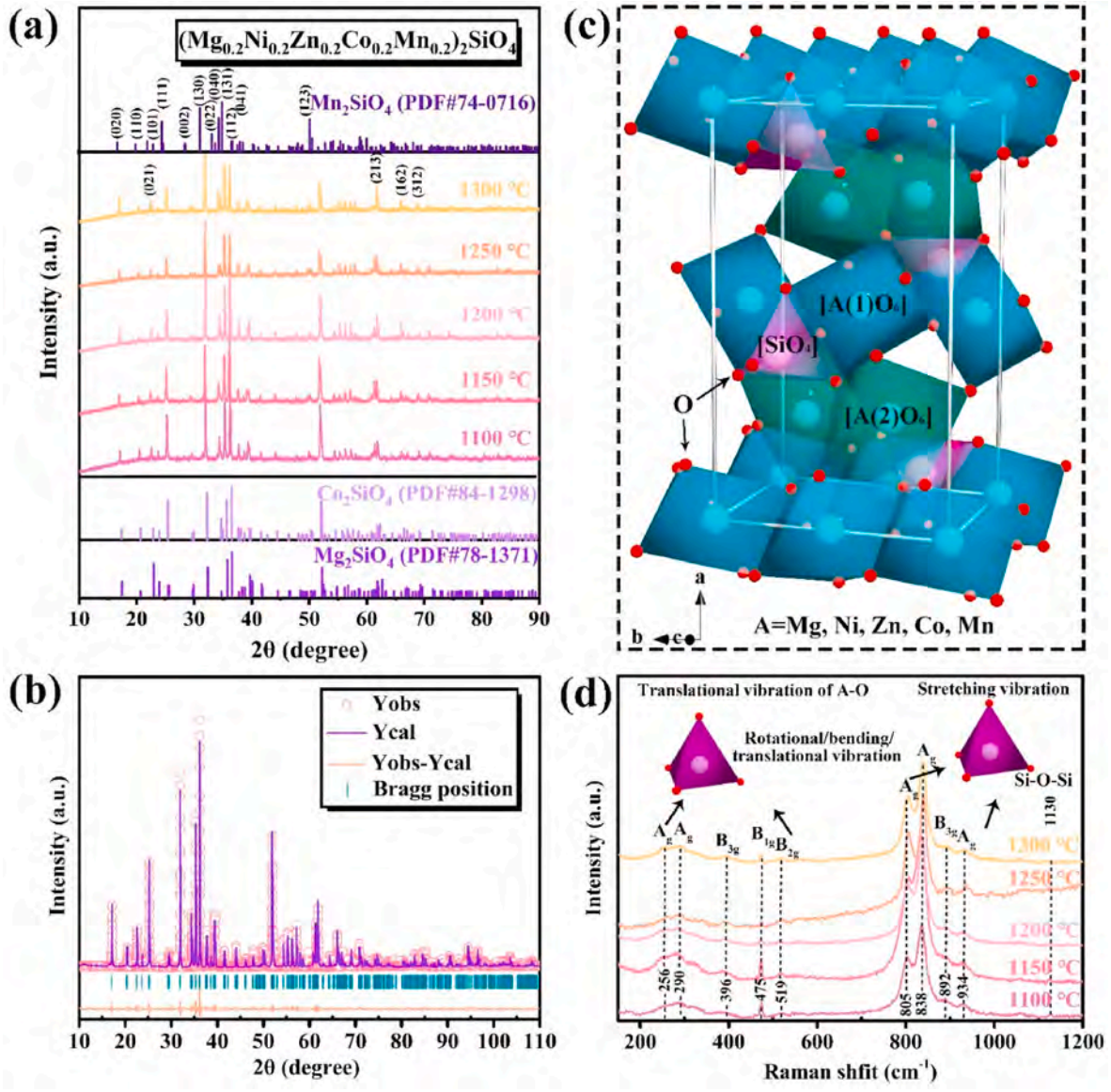

Fig. 2. (a) XRD Patterns of A5SO high-entropy ceramics at different sintering temperatures, (b) Rietveld refinement pattern of A5SO high-entropy ceramic sintered at 1250 °C for 8 h, (c) schematic diagram of the crystal structure of A5SO high-entropy ceramics, and (d) Raman spectra of A5SO high-entropy ceramic sintered at 1250 °C for 8 h.

Table 1
Refined lattice parameters of A5SO and the corresponding theoretical density, as well as the data of A_2SiO_4 (A = Mg, Ni, Co, Zn, Mn) obtained from the PDF standard card and reference.

Material	*a* (Å)	*b* (Å)	*c* (Å)	*α* (°)	*V* (Å^3)	Structure	*d* (g/cm^3)	Source
Mg_2SiO_4	4.7550	10.1960	5.9809	90	290.0	Orthorhombic	3.222	PDF#-78-1371
Ni_2SiO_4	4.7750	10.2160	5.9710	90	291.3	Orthorhombic	4.777	PDF#83-1740
Co_2SiO_4	4.7810	10.2960	5.9980	90	295.3	Orthorhombic	4.722	PDF#84-1298
Zn_2SiO_4	4.7900	10.3000	6.0200	90	297.0	Orthorhombic	4.683	[33]
Mn_2SiO_4	4.9023	10.5964	6.2567	90	325.0	Orthorhombic	4.126	PDF#74-0716
A5SO	4.7762	10.3609	6.0384	90	298.8	Orthorhombic	4.377	This work

$\alpha = \beta = \gamma = 90°$, and its theoretical density is 4.377 g/cm^3. The crystal structure of olivine-type A5SO is shown in Fig. 2(c), which is consistent with Mg_2SiO_4 [32]. It consists of [SiO_4] tetrahedra and [A(1/2)O_6] (A = Mg, Ni, Co, Zn, Mn) octahedra, with Mg, Ni, Co, Zn, and Mn occupying the A site uniformly and randomly. The adjacent A(1)O_6 octahedral units share the oxygen edges of the adjacent octahedra to form chains, while the A(2)O_6 octahedral units form networks by sharing oxygen atoms from the adjacent octahedra. Isolated [SiO_4] tetrahedra is surrounded by [A(1/2)O_6] octahedra, occupying positions with two different symmetries.

Raman spectroscopy is an effective method to reflect the phase structure, cation distribution, and defects via detecting the bond vibration characteristics. Fig. 2(d) illustrates the Raman spectra of A5SO at different sintering temperatures. The theoretical spectral number of Mg_2SiO_4 with the space group of *Pbnm* is 36, A5SO high-entropy ceramics with the same space group also show similar Raman vibrational

modes [34,35]. The characterization results display that only 10 Raman diffraction peaks are detected for the A5SO high-entropy ceramics. The actual measured spectral number of Raman modes were less than the theoretical number due to factors such as low intensity, peak overlay, background, and overtone that affect the properties at a given frequency [36]. The Raman characteristic peaks located between 200 and 550 cm^{-1} are generated by the A-O (A = Mg, Ni, Co, Zn, Mn) translational vibrations and the translational, bending, and rotational vibrations of the [SiO_4] tetrahedra. The Raman peaks at 800-1000 cm^{-1} is generated by the stretching vibration of SiO_4 tetrahedra. Located at 1130 cm^{-1} is generated via the Si–O–Si vibration. The Raman spectroscopy results also verify the successful preparation of A5SO high-entropy ceramics.

3(a)-(e) show the microscopic morphology of the A5SO high-entropy ceramics at different sintering temperatures. The grain size increases gradually with the increase of the sintering temperature, which is one of the reasons for promoting the densification of the samples. Fig. 3(f) plots the apparent density and relative density of the samples with sintering temperature. Their apparent density and the relative density first increase and then decrease with the growth of sintering temperature. The maximum relative density (95.1%) was obtained after sintering of the A5SO high-entropy ceramic at 1250 °C, the corresponding apparent density is 4.161 g/cm^3.

Fig. 4(a) demonstrates the variation in ε_r of the A5SO high-entropy ceramic with the sintering temperature. When the sintering temperature increases from 1100 °C to 1250 °C, the ε_r value increases from 6.50 to 8.02. It drops to 7.63 when the sintering temperature reaches 1300 °C. The variation trend of ε_r is consistent with the denseness. According to the Bosman-Havinga eq.

$$\varepsilon_{corr.} = \varepsilon_r(1 + 1.5p) \tag{3}$$

Among them, $\varepsilon_{corr.}$ is the corrected permittivity, p is the fractional porosity, and the porosity will affect ε_r [36,37]. The $\varepsilon_{corr.}$ is 8.61 for the A5SO high-entropy ceramic sintered at 1250 °C, and the correction value is higher than the measured value. Shannon proposed that the ionic polarizability affects the permittivity and that the molecular polarizability (α) of the compound can be estimated by summing ionic polarizability over the constituent ions [38]. A5SO high-entropy ceramics is calculated as follows:

$$\alpha_{A5SO} = (\alpha_{Mg^{2+}} + \alpha_{Ni^{2+}} + \alpha_{Co^{2+}} + \alpha_{Zn^{2+}}\ \alpha_{Mn^{2+}}) \times 0.2 \times 2 + \alpha_{Si^{4+}}\ 4\alpha_{O^{2-}} = 12.462\ \text{Å}^3 \tag{4}$$

where the ionic polarizabilities of Mg^{2+}, Ni^{2+}, Co^{2+}, Zn^{2+}, Mn^{2+}, Si^{4+}, and O^{2-} are 1.32 $Å^3$, 1.23 $Å^3$, 1.65 $Å^3$, 2.04 $Å^3$, 2.64 $Å^3$, 0.87 $Å^3$, and 2.01 $Å^3$, respectively [38]. The theoretical permittivity ($\varepsilon_{th.}$) was calculated by the Clausius-Mosotti (C-M) eq. with the following [39]:

$$\varepsilon_{th.} = \frac{3V + 8\pi\alpha}{3V - 4\pi\alpha} \tag{5}$$

where V is the volume of a single A5SO particle cell, $V = 298.8/4 = 74.7$ $Å^3$. The calculated ε_r is 7.96, which is very close to the actual measured value (ε_r = 8.02, 1250 °C sintering). This also reaffirms the successful preparation of A5SO high-entropy dielectric ceramics.

The complex chemical bonding theory (P–V-L theory) allows the calculation of the magnitude of the bond ionicity (f_i), and thus the inferring the contribution of different chemical bonds to the ε_r. The crystal structure of A5SO high-entropy ceramics needs to be decomposed as the sum of the diatomic expression A_mB_n (A is the cation and B is the anion) to implement the PVL theory calculation [40,41].

$$\text{A5SO} = \text{A(1)}_{1/3}\text{O(1)}_{1/2} + \text{A(1)}_{1/3}\text{O(2)}_{1/2} + \text{A(1)}_{1/3}\text{O(3)}_{1/2} + \text{A(2)}_{1/6}\text{O(1)}_{1/4} + \text{A(2)}_{1/6}\text{O(2)}_{1/4} + \text{A(2)}_{1/3}\text{O(3)}^1_{1/2} + \text{A(2)}_{1/3}\text{O(3)}^2_{1/2} + \text{Si}_{1/4}\text{O(1)}_{1/4} + \text{Si}_{1/4}\text{O(2)}_{1/4} + \text{Si}_{1/2}\text{O(3)}_{1/2} \tag{6}$$

The bond ionicity (f_i^{μ}) of u chemical bonds can be calculated by the following eqs:

$$f_i^{\mu} = \frac{(C^{\mu})^2}{(E_g^{\mu})^2} \tag{7}$$

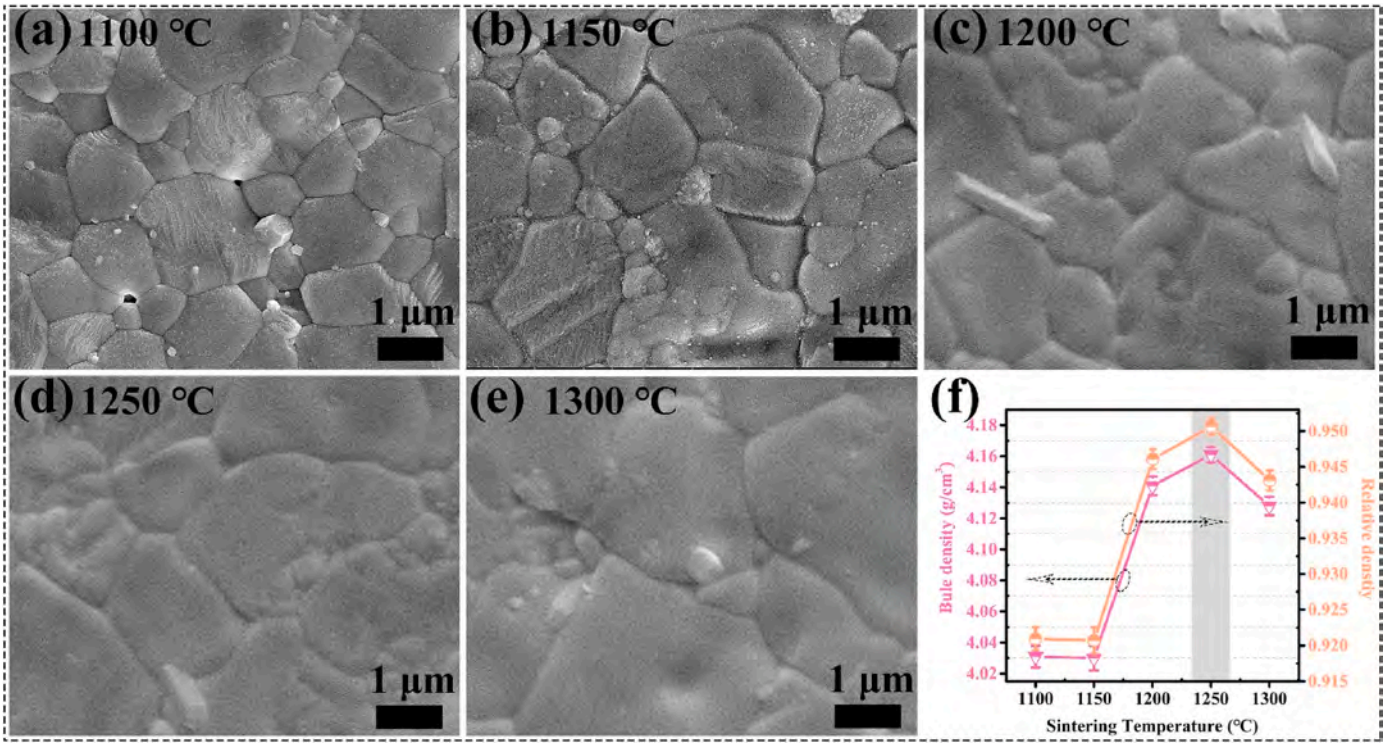

Fig. 3. (a)–(e) are the SEM images of A5SO high-entropy ceramics at different sintering temperatures, and (f) are the apparent densities and relative densities at different sintering temperatures.

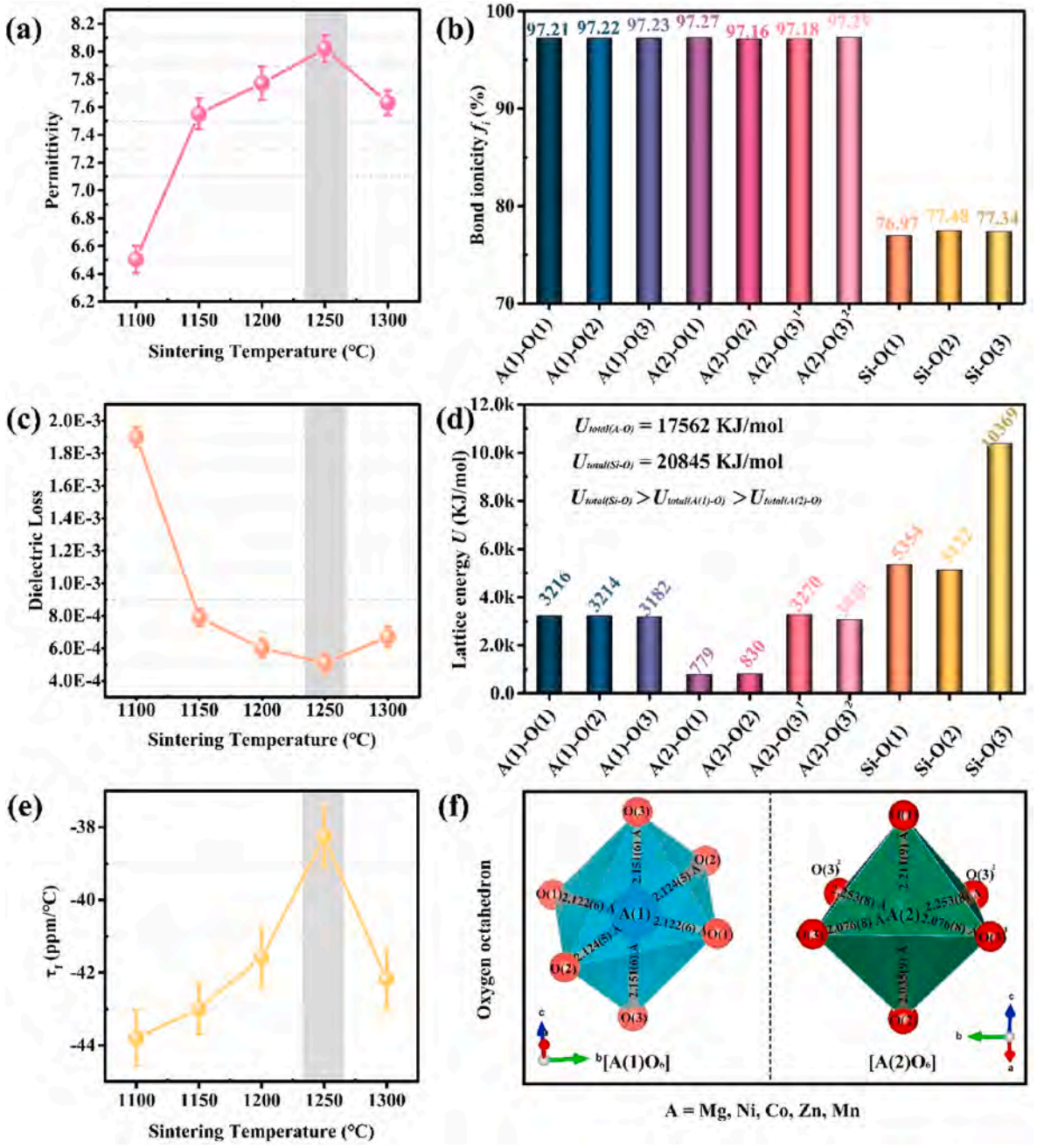

Fig. 4. The variation patterns of (a) permittivity, (c) dielectric loss, and (e) τ_f with sintering temperature for A5SO high-entropy ceramics. (b) The chemical bond ionicity, (d) calculated lattice energy, and (f) schematic diagram of oxygen octahedra of A5SO high-entropy ceramics sintered at 1250 °C for 8 h.

$$(E_g^\mu)^2 = (E_h^\mu)^2 + (C^\mu)^2 \tag{8}$$

$$(E_h^\mu)^2 = \frac{39.74}{(d^\mu)^{2.48}} \tag{9}$$

$$C^\mu = 14.4 b^\mu e^{(-k_s^\mu r_o^\mu)}\left[\frac{(Z_A^\mu)^*}{r_o^\mu} - \frac{n}{m}\frac{(Z_B^\mu)^*}{r_o^\mu}\right],\ n \geq m \tag{10}$$

where, E_g^μ is the average energy gap between the molecular orbital and the antibonding molecular orbital, and E_h^μ, C^μ represent the homopolar and heteropolar parts of the energy gap, respectively. d^μ is the bond length of the chemical bond of μ, and b^μ is the correction factor. $\exp(-k_s^\mu r_o^\mu)$ is the Thomas-Fermi shielding factor, and $(Z_A^\mu)^*$, $(Z_B^\mu)^*$ represent the effective valence electron numbers of A, B [37]. In addition, the calculation formula of each parameters in the relevant eq. (10) are listed in SI (Supplementary Information). The ionicity of the different chemical bonds in A5SO high-entropy ceramics is shown in Fig. 4(b) (detailed values are listed in Table S1 in SI), and the ionicity values of the A-O bonds account for the major part of the ionicity of the chemical bonds. Therefore, the ε_r of A5SO high-entropy ceramics is mainly influenced by the ionicity of the A-O bond.

Fig. 4(c) shows the variation of dielectric loss with sintering temperature, which follows the same trend as ε_r, reaching the lowest value of 0.00051 at 1250 °C (at 14.5 GHz). The A5SO high-entropy ceramics did not generate heterogeneous phases, and the effect of the heterogeneous phase on dielectric loss is not considered. The A5SO ceramics sintered at 1100 °C, 1150 °C, 1200 °C, and 1300 °C showed higher dielectric loss due to their densities below 95%. The specific dielectric loss values for all samples are listed in Table 2. Density and

Table 2
The dielectric loss values of A5SO high-entropy ceramics at different sintering temperatures.

Sintering temperature (°C)	Dielectric loss
1100	0.0019
1150	0.00079
1200	0.00060
1250	0.00051
1300	0.00067

heterogeneous phases, which are factors affecting dielectric loss values, are negligible for samples with densities higher than 95%. The effect of the binding capacity of cations and oxygen ions on microwave dielectric loss can be analyzed using lattice energy [42]. If the crystal has high binding energy, the intrinsic loss will be reduced. The calculation equation is as follows:

$$U_{cal} = \sum_{\mu}(U_{bc}^{\mu} + U_{bi}^{\mu}) \tag{11}$$

$$U_{bc}^{\mu} = 2100m\frac{(Z_{+}^{\mu})^{1.64}}{(d^{\mu})^{0.75}}f_{c}^{\mu} \tag{12}$$

$$U_{bi}^{\mu} = 1270\frac{(m+n)Z_{+}^{\mu}Z_{-}^{\mu}}{d^{\mu}}(1-\frac{0.4}{d^{\mu}})f_{i}^{\mu} \tag{13}$$

U_{bi}^{μ}, U_{bc}^{μ} are the lattice energies of ionic and covalent contributions, respectively. Z_{+}^{μ}, Z_{-}^{μ} denote the chemical bonding valence presented by cations and anions in the chemical bond μ. The calculated results are plotted in Fig. 4(d), and the specific lattice energy values are listed in Table S1. The results illustrate that the stacking lattice energies of the A-O and Si–O bonds are similar, indicating that both affect the dielectric loss of A5SO.

Fig. 4(e) shows the variation of τ_f value with sintering temperature for A5SO high-entropy ceramics. The best τ_f value is exhibited with −38.2 ppm/°C at 1250 °C as with the variation of ε_r and dielectric loss. The τ_f of most microwave dielectric ceramics is affected by their crystal structure, especially the oxygen octahedral distortion [30,43]. The distortion of the [AO_6] octahedron is caused by the random occupation of the a-site of the A5SO high-entropy ceramic by five atoms of Mg, Ni, Co, Zn, and Mn. The octahedral distortion ($\Delta octa.$) is calculated by the following eq.

$$\triangle_{octa.} = \frac{1}{6}\sum_{i}(\frac{R_{i-o}-R_{av.}}{R_{av.}})^2 \tag{14}$$

where R_{i-o} is the bond length of the i-O bond, and $R_{av.}$ is the average bond length. The aberrations were calculated for the [$A(1)O_6$] octahedron and the [$A(2)O_6$] octahedron, and the results are listed in Table 3. The structures of the two types of oxygen octahedra are schematically plotted in Fig. 4(f), and the specific key length information can be obtained from it. At the same time, Table 3 also counts some of the oxygen octahedra distortion information with the numerical magnitude of τ_f. It is obvious that the value of τ_f is almost zero for materials with little oxygen octahedral distortion based on the comparison results. The A5SO ceramics has a relatively significant degree of [$A(2)O_6$] oxygen octahedral distortion in this study, which leads to a τ_f value of −38.2 ppm/°C. Overall, the introduction of the high entropy concept improves the stability of the structure and reduces the degree of oxygen octahedral distortion.

4. Conclusions

In this study, $(Mg_{0.2}Ni_{0.2}Zn_{0.2}Co_{0.2}Mn_{0.2})_2SiO_4$ high-entropy dielectric ceramics were prepared via the solid-phase method. The phase structure, vibrational properties, microscopic morphology, and chemical bonding properties of $(Mg_{0.2}Ni_{0.2}Zn_{0.2}Co_{0.2}Mn_{0.2})_2SiO_4$ high-entropy dielectric ceramics were analyzed by XRD, Raman, SEM-EDX, and complex chemical bonding theory concerning their dielectric properties. The results show that the best dielectric properties (ε_r is 8.02, dielectric loss is 0.00051 at 14.5 GHz, and τ_f is −38.2 ppm/°C) were obtained by sintering at 1250 °C for 8 h. According to the complex chemical bonding theory, it is known that the ε_r of A5SO high-entropy ceramic is mainly affected by the A-O bonding, while the dielectric loss is affected by both A-O and Si–O, due to the close lattice energy of both. Due to the relatively large distortion parameters of the [$A(2)O_6$] oxygen octahedron, which makes the τ_f of this high-entropy ceramic −38.2 ppm/°C.

Table 3
Information on τ_f and oxygen octahedron of microwave dielectric ceramics.

Material	Crystal structure	Oxygen octahedron	Octahedral distortion ($\Delta_{octa.}$)	τ_f (ppm/°C)	Refs.
A5SO-1250 °C	Olivine	[$A(1)O_6$]	3.9×10^{-5}	−38.2	This work
		[$A(2)O_6$]	1.8×10^{-3}		
A5SO-1100 °C		[$A(1)O_6$]	9.6×10^{-4}	−43.8	
		[$A(2)O_6$]	6.8×10^{-3}		
A5SO-1150 °C		[$A(1)O_6$]	7.3×10^{-5}	−42.9	
		[$A(2)O_6$]	5.2×10^{-3}		
A5SO-1200 °C		[$A(1)O_6$]	5.4×10^{-5}	−41.6	
		[$A(2)O_6$]	3.6×10^{-3}		
A5SO-1300 °C		[$A(1)O_6$]	7.2×10^{-5}	−42.1	
		[$A(2)O_6$]	4.7×10^{-3}		
$Co_{0.5}Ti_{0.5}TaO_4$	Trirutile	[Co/Ta^1O_6]	$\sim3.3\times10^{-2}$	114.54	[44]
		[Co/Ta^2O_6]	$\sim2.7\times10^{-4}$		
$LiYbSiO_4$	Olivine	[LiO_6]	1.37×10^{-4}	+4.52	[45]
		[YbO_6]	7.5×10^{-4}		
$LiRGeO_4$	Olivine	[RO_6]	5.0×10^{-4}	−2.9	[30]

Declaration of competing interest

The authors declare that they have no known competing financial interests or personal relationships that could have appeared to influence the work reported in this paper.

Acknowledgments

We sincerely appreciate the projects supported by the National Natural Science Foundation of China (Grant No.51902042), the National Key Scientific Instrument and Equipment Development Project (No. 51827802), and the Major Science and Technology Specific Projects of Sichuan Province (No. 2019ZDZX0026).

Appendix A. Supplementary data

Supplementary data to this article can be found online at https://doi.org/10.1016/j.ceramint.2022.04.317.

References

[1] D.W. Wang, S.Y. Zhang, G. Wang, Y. Vardaxoglou, W. Whittow, D. Cadman, D. Zhou, K.X. Song, I.M. Reaney, Cold sintered $CaTiO_3$ - K_2MoO_4 microwave dielectric ceramics for integrated microstrip patch antennas, Appl. Mater. Today 18 (2020) 100519.
[2] M.W. Lufaso, Crystal structures, modeling, and dielectric property relationships of 2:1 ordered $Ba_3MM'_2O_9$ (M: Mg, Ni, Zn; M′: Nb, Ta) perovskites, Chem. Mater. 16 (2004) 2148–2156.
[3] T. Joseph, M.T. Sebastian, Dielectric properties of $(Sr_{1-x}A_x)_2(Z_{n1-x}B_x)Si_2O_7$ ceramics (A=Ca, Ba and B=Co, Mg, Mn, Ni), J. Am. Ceram. Soc. 93 (2010) 147–154.
[4] D. Zhou, L.X. Pang, D.W. Wang, Z.M. Qi, I.M. Reaney, High quality factor, ultralow sintering temperature $Li_6B_4O_9$ microwave dielectric ceramics with ultralow density for antenna substrates, ACS Sustain. Chem. Eng. 6 (2018) 11138–11143.
[5] L.X. Pang, D. Zhou, D.W. Wang, J.X. Zhao, W.G. Liu, Z.X. Yue, I.M. Reaney, Temperature stable $K_{0.5}(Nd_{1-x}Bi_x)_{0.5}MoO_4$ microwave dielectrics ceramics with ultra-low sintering temperature, J. Am. Ceram. Soc. 101 (2018) 1806–1810.

[6] K.X. Song, P. Liu, H.X. Lin, W.T. Su, J. Jiang, S. Wu, Z.H. Ying, H.B. Qin, Symmetry of hexagonal ring and microwave dielectric properties of $(Mg_{1-x}Ln_x)_2Al_4Si_5O_{18+x}$ (Ln=La, Sm) cordierite-type ceramics, J. Eur. Ceram. Soc. 36 (2016) 1167–1175.

[7] J.B. Song, K.X. Song, J.S. Wei, H.X. Lin, J. Wu, J.M. Xu, W.T. Su, Z.Q. Chen, Ionic occupation, structures, and microwave dielectric properties of $Y_3MgAl_3SiO_{12}$ garnet - type ceramics, J. Am. Ceram. Soc. 101 (2018) 244–251.

[8] L. Li, C.H. Liu, J.Y. Zhu, X.M. Chen, B_2O_3-modified fused silica microwave dielectric materials with ultra-low dielectric constant, J. Eur. Ceram. Soc. 35 (2015) 1799–1805.

[9] D. Zhou, C.A. Randall, L.X. Pang, H. Wang, J. Guo, G.Q. Zhang, X.G. Wu, L. Shui, X. Yao, Microwave dielectric properties of Li_2WO_4 ceramic with ultra-low sintering temperature, J. Am. Ceram. Soc. 94 (2011) 348–350.

[10] X. Zhou, L.T. Liu, J.J. Sun, N.K. Zhang, H.Z. Sun, H.T. Wu, W.H. Tao, Effects of $(Mg_{1/3}Sb_{2/3})^{4+}$ substitution on the structure and microwave dielectric properties of $Ce_2Zr_3(MoO_4)_9$ ceramics, J. Adv. Ceram. 10 (2021) 778–789.

[11] C. Feng, X. Zhou, B.J. Tao, H.T. Wu, S.F. Huang, Crystal structure and enhanced microwave dielectric properties of the $Ce_2[Zr_{1-x}(Al_{1/2}Ta_{1/2})_x]_3(MoO_4)_9$ ceramics at microwave frequency, J. Adv. Ceram. 11 (2022) 392–402.

[12] H.R. Tian, J.J. Zheng, L.T. Liu, H.T. Wu, H. Kimura, Y.Z. Lu, Z.X. Yue, Structure characteristics and microwave dielectric properties of $Pr_2(Zr_{1-x}Ti_x)_3(MoO_4)_9$ solid solution ceramic with a stable temperature coefficient, J. Mater. Sci. Technol. 116 (2022) 121–129.

[13] J.W. Yeh, S.K. Chen, S.J. Lin, J.Y. Gan, T.S. Chin, T.T. Shun, C.H. Tsau, S.Y. Chang, Nanostructured high-entropy alloys with multiple principal elements: novel alloy design concepts and outcomes, Adv. Eng. Mater. 6 (2004) 299–303.

[14] B. Cantor, I. Chang, P. Knight, A.J.B. Vincent, Microstructural development in equiatomic multicomponent alloys, Mat. Sci. Eng. A Struct. 375–377 (2004) 213–218.

[15] M.H. Chuang, M.H. Tsai, W.R. Wang, S.J. Lin, J.W. Yeh, Microstructure and wear behavior of $Al_xCo_{1.5}CrFeNi_{1.5}Ti_y$ high-entropy alloys, Acta Mater. 59 (2011) 6308–6317.

[16] Z.M. Li, K.G. Pradeep, Y. Deng, D. Raabe, C.C. Tasan, Metastable high-entropy dual-phase alloys overcome the strength-ductility trade-off, Nature 534 (2016) 227–230.

[17] C.M. Rost, E. Sachet, T. Borman, A. Moballegh, E.C. Dickey, D. Hou, J.L. Jones, S. Curtarolo, J.P. Maria, Entropy-stabilized oxides, Nat. Commun. 6 (2015) 8485.

[18] R.Z. Zhang, M.J. Reece, Review of high entropy ceramics: design, synthesis, structure and properties, J. Mater. Chem. 7 (2019) 22148–22162.

[19] L. Backman, J. Gild, J. Luo, E.J. Opila, Part I: theoretical predictions of preferential oxidation in refractory high entropy materials, Acta Mater. 197 (2020) 20–27.

[20] R. Feng, P.K. Liaw, M.C. Gao, M. Widom, First-principles prediction of high-entropy-alloy stability, npj Comput. Mater. 3 (2017) 50.

[21] C. Oses, C. Toher, S. Curtarolo, High-entropy ceramics, Nat. Rev. Mater. 5 (2020) 295–309.

[22] K.X. Song, X.M. Chen, X.C. Fan, Effects of Mg/Si ratio on microwave dielectric characteristics of forsterite ceramics, J. Am. Ceram. Soc. 90 (2010) 1808–1811.

[23] J. Sugihara, K. Kakimoto, I. Kagomiya, H. Ohsato, Microwave dielectric properties of porous Mg2SiO4 filling with TiO_2 prepared by a liquid phase deposition process, J. Eur. Ceram. Soc. 27 (2007) 3015–3108.

[24] H.C. Xiang, C.C. Li, H. Jantunen, L. Fang, A.E. Hill, Ultralow loss $CaMgGeO_4$ microwave dielectric ceramic and its chemical compatibility with silver electrodes for low-temperature cored ceramic applications, ACS Sustain. Chem. Eng. 6 (2018) 6458–6466.

[25] A. Rose, B. Masin, H. Sreemoolanadhan, K. Ashok, T. Vijayakumar, Synthesis and microwave dielectric studies of pure Li2MgSiO4 and B2O3, MgF2, WO3 added Li2MgSiO4 for substrate applications, Appl. Surf. Sci. 449 (2018) 96–104.

[26] M.F. Zhong, H. Su, X.L. Jing, Y.X. Li, Q.H. Lu, Y.L. Jing, Crystal structure and microwave dielectric properties of $Li_2Mg_{0.6}CoZn_{0.4}SiO_4$ ceramic for LTCC applications, Ceram. Int. 9 (2020) 13095–13101.

[27] R. Peng, Y.X. Li, X.L. Tang, Y.C. Lu, Q. Zhang, X.Y. Wang, H. Su, Improved sintering and microwave dielectric properties of Li_2CaSiO_4 ceramic with magnesium atom substitution, Ceram. Int. 46 (2020) 8869–8876.

[28] Y. Tang, M.Y. Xu, L. Duan, J.Q. Chen, C.C. Li, H.C. Xiang, L. Fang, Structure, microwave dielectric properties, and infrared reflectivity spectrum of olivine type Ca_2GeO_4 ceramic, J. Eur. Ceram. Soc. 39 (2019) 2354–2359.

[29] C.C. Li, H.C. Xiang, M.Y. Xu, Y. Tang, L. Fang, Li_2AGeO_4 (A = Zn, Mg): two novel low-permittivity microwave dielectric ceramics with olivine structure, J. Eur. Ceram. Soc. 38 (2017) 1524–1528.

[30] H.C. Xiang, L. Yao, J.Q. Chen, A.H. Yang, H.T. Yang, L. Fang, Microwave dielectric high-entropy ceramic $Li(Gd_{0.2}Ho_{0.2}Er_{0.2}Yb_{0.2}Lu_{0.2})GeO_4$ with stable temperature coefficient for low-temperature cofired ceramic technologies, J. Mater. Sci. Technol. 93 (2021) 28–32.

[31] B.W. Hakki, P.D. Coleman, A dielectric-resonator method of measuring inductive capacities in the millimeter wave range, IRE Trans. Microw. Theor. Tech. 8 (1960) 402–410.

[32] Y.M. Lai, X.L. Tang, X. Huang, H.W. Zhang, X.F. Liang, J. Li, H. Su, Phase composition, crystal structure and microwave dielectric properties of $Mg_{2-x}Cu_xSiO_4$ ceramics, J. Eur. Ceram. Soc. 38 (2017) 1508–1516.

[33] S.Z. Karazhanov, P. Ravindran, P. Vajeeston, A.G. Ulyashin, H. Fjellvåg, B. G. Svensson, Phase stability and pressure-induced structural transitions at zero temperature in ZnSiO3 and Zn2SiO4, J. Phys. Condens. Matter 21 (2009) 485801.

[34] E. Kroumova, M.I. Aroyo, J.M. Perez-Mato, A. Kirov, C. Capillas, S. Ivantchev, H. Wondratschek, Bilbao crystallographic server: useful databases and tools for phase-transition studies, Phase Transitions 76 (2003) 155–170.

[35] Y.M. Lai, X.L. Tang, H.W. Zhang, X.F. Liang, X. Huang, H. Su, Correlation between structure and microwave dielectric properties of low- temperature-fired Mg_2SiO_4 ceramics, Mater. Res. Bull. 99 (2018) 496–502.

[36] A.J. Bosman, E.E. Having, Temperature dependence of dielectric constants of cubic ionic compounds, Phys. Rev. 129 (1963) 1593–1600.

[37] I.D. Brown, R.D. Shannon, Empirical bond-strength–bond-length curves for oxides, Acta Crystallogr. A 29 (1973) 266–282.

[38] R.D. Shannon, Dielectric polarizabilities of ions in oxides and fluorides, J. Appl. Phys. 73 (1993) 348–366.

[39] P.V. Rysselberghe, Remarks concerning the clausius-mossotti law, J. Phys. Chem. 36 (1932) 1152–1155.

[40] Z. Ping, Y.G. Zhao, X. Wang, The relationship between bond ionicity, lattice energy, coefficient of thermal expansion and microwave dielectric properties of Nd $(Nb_{1-x}Sb_x)O_4$ ceramics, Dalton Trans. 44 (2015) 10932–10938.

[41] B.F. Levine, Bond susceptibilities and ionicities in complex crystal structures, J. Chem. Phys. 59 (1973) 1463–1486.

[42] E.S. Kim, B.S. Chun, R. Freer, R.J. Cernik, Effects of packing fraction and bond valence on microwave dielectric properties of $A^{2+}B^{6+}O_4$ (A^{2+}: Ca, Pb, Ba; B^{6+}: Mo, W) ceramics, J. Eur. Ceram. Soc. 30 (2010) 1731–1736.

[43] J. Li, X.K. Lan, K. Du, X.Q. Song, W.Z. Lu, G.F. Fan, W. Lei, Crystal structure and temperature dependence of permittivity in barium aluminate based solid solutions, J. Am. Ceram. Soc. 102 (2019) 7480–7490.

[44] H.Y. Yang, S.R. Zhang, Y.W. Chen, H.C. Yang, Y. Yuan, E.Z. Li, Crystal chemistry, Raman spectra, and bond characteristics of trirutile-type $Co_{0.5}Ti_{0.5}TaO_4$ microwave dielectric ceramics, Inorg. Chem. 58 (2018) 968–976.

[45] C.X. Su, L.Y. Ao, Z.W. Zhang, Y.F. Zhai, J.Q. Chen, Y. Tang, L.J. Liu, L. Fang, Crystal structure, Raman spectra and microwave dielectric properties of novel temperature-stable $LiYbSiO_4$ ceramics, Ceram. Int. 46 (2020) 19996–20003.